Biomed Microdevices (2015) 17:74
DOI 10.1007/s10544-015-9980-7

Wireless programmable electrochemical drug delivery micropump with fully integrated electrochemical dosing sensors

Roya Sheybani[1] · Angelica Cobo[1] · Ellis Meng[1,2]

Abstract We present a fully integrated implantable electrolysis-based micropump with incorporated EI dosing sensors. Wireless powering and data telemetry (through amplitude and frequency modulation) were utilized to achieve variable flow control and a bi-directional data link with the sensors. Wireless infusion rate control (0.14–1.04 μL/min) and dose sensing (bolus resolution of 0.55–2 μL) were each calibrated separately with the final circuit architecture and then simultaneous wireless flow control and dose sensing were demonstrated. Recombination detection using the dosing system, as well as, effects of coil separation distance and misalignment in wireless power and data transfer were studied. A custom-made normally closed spring-loaded ball check valve was designed and incorporated at the reservoir outlet to prevent backflow of fluids as a result of the reverse pressure gradient caused by recombination of electrolysis gases. Successful delivery, infusion rate control, and dose sensing were achieved in simulated brain tissue.

Keywords Electrolysis micropump · Electrochemical sensors · Patient-tailored drug delivery · Dosing accuracy · Check valve

✉ Ellis Meng
ellis.meng@usc.edu

[1] Department of Biomedical Engineering, Viterbi School of Engineering, University of Southern California, 1042 Downey Way, DRB-140, Los Angeles, CA 90089-1111, USA

[2] Department of Electrical Engineering, Viterbi School of Engineering, University of Southern California, 3651 Watt Way, VHE-602, Los Angeles, CA 90089-0241, USA

1 Introduction

Effective drug therapy is an essential tool in the treatment and management of chronic conditions such as pain, spasticity, hypertension, respiratory disease, and diabetes (Menehan 2006). In the most severe cases, patients suffering from these conditions are implanted with commercially-available drug infusion pumps for therapeutic management. These devices bypass physiological barriers to enable delivery of new compounds such as biologics, biosimilars, and other small molecules directly to the target tissue (Urquhart et al. 1984; Urquhart 2001); and thereby maximize therapeutic efficacy of the drug and limiting toxic side effects by delivering the correct amount of drug in the vicinity of the target cells and reducing the drug exposure to the nontarget cells (Fiering et al. 2009).

However, according to reports by the US Food and Drug Administration (FDA), over a 5 year period, of the 56,000 medical device reports relating to the use of infusion pumps, approximately 65 % were related to system malfunctions (Trombly 2012). Unfortunately, these systems did not incorporate closed-loop feedback sensors that could ensure that the correct dose and flow rate are delivered resulting in late diagnosis of malfunction until physiological signs are reported by the patient. This could potentially lead to serious health complications, injury, or even death (FDA: US Food and Drug Administration 2011, 2011, 2011, 2012). As such, there is a fundamental unmet need with regards to implantable drug delivery pumps for sensors that verify accuracy of delivery and confirm dosage. The inclusion of sensors to track the delivered dose volume and flow rate and report to the user the state of the pump in real-time allows for active control over the delivery profile. This will lead to improved patient care by confirming the correct delivery of the right drug dose to the desired therapy location. It has been shown that

Published online: 07 July 2015

controlled administration of drugs can increase drug therapy effectiveness, in some cases up to 60 % (Tng et al. 2012).

On the other hand, most commercially available pumps for site-specific delivery are based on decades-old mechanisms that only provide constant infusion rate. While certain chronic conditions, such as drug addiction and menopause, have associated static therapeutic windows and may be treated with constant drug administration (Bruguerolle and Labrecque 2007), most chronic conditions have chronobiological pattern in their pathogenesis (Halberg et al. 1973; Hrushesky 1990; Halberg et al. 1992; Lis et al. 2003; Youan 2004). More importantly, drug dosing affects the therapeutic window. Following successful drug administration, the clinical need for additional pharmacological intervention for certain conditions diminishes transiently while the risk of side effects dramatically increases (Meng and Hoang 2012). Programmable drug delivery devices would allow for therapies and administration regimens that mimic the chronobiological pattern of the condition (Paolino et al. 2006). Sensors incorporated within these programmable devices can not only be used to ensure dosing accuracy and report system malfunctions in real time; monitoring the drug release profile could also provide useful information for bioengineers and clinicians to optimize the drug therapy for the patients (Tng et al. 2012).

Previously, the possibility of monitoring fluid delivery using changes in electrochemical impedance (EI) of a fluid container was demonstrated (Sheybani et al. 2012a) followed by integration of these sensors with a wired, electrolysis-based micropump (Sheybani et al. 2013). For implantable pumps, wireless power and data transmission eliminate transcutaneous wires and catheters thereby reducing surgical complexity, improving patient mobility, and allowing drug administration outside of clinical settings. Preliminary proof of concept prototypes for wireless actuator operation (Sheybani and Meng 2014) and wireless sensing were presented (Sheybani and Meng 2015). Here, an advanced integrated system is presented that for the first time utilizes wireless powering and data telemetry simultaneously to achieve programmable closed-loop drug delivery. The micropump reservoir was redesigned to minimize inaccessible dead volume to less than 100 μL without altering the deliverable volume. A normally closed micromechanical spring-loaded ball was custom-made and incorporated at the micropump reservoir outlet to prevent backflow of fluids as a result of the reverse pressure gradient caused by recombination of electrolysis gases. Ferrite cores were added to the internal receiving and transmitting coils, to allow for increased pickup and miniaturization, without increasing the micropump footprint. Device design and fabrication of the electrochemical pump and sensors, as well as, wireless architecture are presented in detail. Wireless programming and sensing were each calibrated, followed by demonstration of simultaneous flow control and sensing for an example delivery regimen. Design, fabrication, and characterization of the check valve, along with system operation after the integration of the check valve was presented. Lastly, the effects of coil misalignment and distance and transmission through simulated brain tissue material on wireless power and data transmission were studied.

2 System design and fabrication

2.1 System operation concept and architecture

The schematic diagram of the micropump with integrated dosing sensors is shown in Fig. 1 (a, b). The micropump consisted of an electrolysis based actuator housed in a drug reservoir. Electrochemical pumping was achieved by wireless inductive power transfer resulting in constant current application to a pair of Nafion® coated interdigitated Pt electrodes which converted water into hydrogen and oxygen gases via electrolysis. The resulting volume expansion was then harnessed to inflate the drug-separating bellows which in turn displaced the fluid in the drug chamber and expelled drug through the catheter to the delivery site. Once the current application was ceased, the Pt electrodes catalyzed the recombination of gases into water, enabling repeatable pumping. A custom-made normally closed spring-loaded ball check valve (Fig. 1c) was included at the pump outlet to prevent backflow of fluids as a result of the reverse pressure gradient caused by recombination. A set of refill ports were added to the drug reservoir to allow for transcutaneous refilling of drug after implantation.

Electrochemical dose sensing was achieved through measuring electrochemical impedance by applying a small sinusoidal excitation voltage across a pair of sensor electrodes placed in the drug reservoir. At sufficiently high frequencies, the measured impedance could be directly correlated to the volume of drug remaining in the reservoir. Therefore, changes in reservoir content, delivery flow rate, blockages in the delivery catheter, drug refills, and even damage to the electrolysis chamber could be assessed in real-time and recorded for future analysis using a LabVIEW graphical user interface (GUI).

The overall wireless system architecture is presented in Fig. 2. A class E inductive powering scheme was used to power the micropump as well as the internal circuit components. Once picked up by the internal receiving coil, the signal was fully rectified, fed through a current regulator, and applied to power the actuator. For wireless on-demand control of the infusion rate, amplitude shift keying (ASK) modulation was used to transmit a data signal from the external transmitter to the internal circuit, changing the wiper position of a current setting potentiometer, which in turn altered the current output of a regulator supplying current to the actuator. Pulse width of the data signal determined the number of incremental steps of potentiometer wiper position. ASK modulation was also used

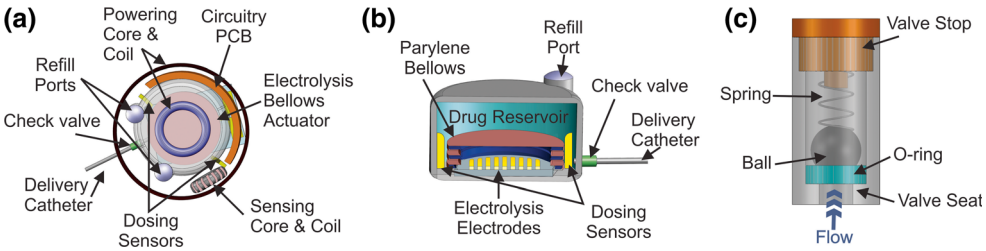

Fig. 1 Schematic diagram: **a** top view micropump with integrated sensors and circuitry, **b** side view cut-out showing the internal components, **c** custom-made normally closed spring-loaded ball check valve

for data transfer for dose sensing. A fixed 500 kHz sensing signal was carried by the power signal through air (and skin when implanted) to the internal circuit. The received signal was applied to the dosing sensors. As the current through the sensors was held constant, changes in sensor impedance resulted in a change in voltage across an n-channel metal–oxide–semiconductor field effect transistor (n-MOSFET), causing a change in its capacitance. As a result, the resonance frequency of the implanted transmitted coil shifted. This shift was reflected on the external receiving coil. The shift in frequency was measured externally and correlated to changes in the reservoir fluid volume. To further improve the sampling speed and signal quality, the externally received signal was amplified and multiplied by the original transmitted signal.

A Parallax Board of Education USB carrier board kit, a Basic Stamp 2 Module microcontroller, and an Easy Bluetooth Module (Parallax Inc., Rocklin, CA) were used to control wireless signal transmission from the external module to the internal circuit via Bluetooth. An analog input high speed data acquisition module (2 MSamples/s; NI USB-6366, National Instruments, Austin, TX) was used to record the externally received sensor data. LabVIEW (v 2009, National Instruments, Austin, TX) and Basic Stamp 2 Editor (v. 2.5.2) were used to program the communication and signal processing.

2.2 Fabrication and circuit layout

The bellows actuator can only displace the column of fluid directly above it; as such the fluid around the bellows (between bellows outer diameter and reservoir inner wall) cannot be accessed for pumping and is considered dead volume which should be minimized. By designing a reservoir with an inner diameter close to that of the bellows outer diameter, the dead volume between was minimized to less than 100 μL (Gensler 2013; Cobo et al. (2015).

Reservoir packaging was designed and fabricated from USP class VI DSM Somos® WaterShed XC 11122, an optically clear, water resistant material similar to the common thermoplastic acrylonitrile butadiene styrene (ABS), using stereolithography (FineLine Prototyping, Inc., Raleigh, NC), a high resolution rapid prototyping technique. Two vertical indentations and access ports were incorporated in the reservoir wall to allow for the integration of dosing sensors. The new reservoir featured two silicone-filled refill ports (10:1 base-to-curing agent ratio Class VI MDX-4 4210; Factor II, Lakeside, AZ), as well as a silicone catheter (ID. 1.016 mm, OD 2.159 mm, VWRbrand Select Silicone Tubing, VWR International, Radnor, PA).

For the electrolysis actuator, interdigitated Pt electrodes (100 μm wide elements separated by 100 μm gaps, 8 mm diameter footprint) were fabricated on polyetheretherketone (PEEK) sheets (thickness of 0.5 mm, CS Hyde, Lake Villa, IL) by a liftoff method. Electrodes fabricated on PEEK were chosen due to reduce overall weight (0.112 vs. 0.260 g) and improved electrolysis efficiency (an average of 8.15 %) compared to electrodes fabricated on borosilicate glass (Sheybani and Meng 2012). Individual electrodes were separated and dip coated with Nafion® (Dupont DE521 Solution, Ion Power, INC, New Castle, DE) twice. Kynar™ silver plated copper wires (30 AWG, Jameco Electronics, Belmont, CA) were soldered to contact pads on the electrodes. The joint was strengthened and insulated with nonconductive marine epoxy (Loctite, Westlake, OH) (Sheybani and Meng 2012). Parylene

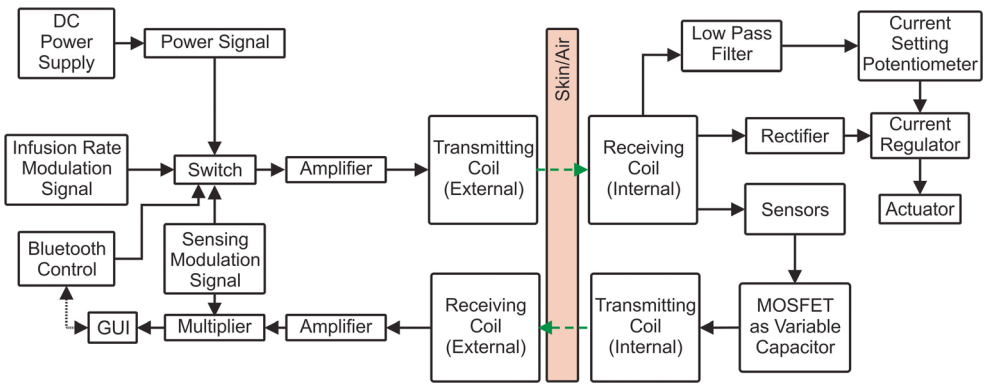

Fig. 2 System architecture of wireless power and sensing system

bellows (2 convolutions; 10 mm outer diameter, 6 mm inner diameter) were fabricated as described in (Gensler et al. 2011) using a mold formed from stacked silicone rubber sheets (10:1 base-to-curing agent ratio Sylgard 184, Dow Corning, Midland, MI) and molten (~50 °C) polyethylene glycol (PEG; 1000 MW, Sigma Aldrich, St. Louis, MO). A 13.5 μm layer of Parylene C (Specialty Coatings Systems, Indianapolis, IN) was deposited over the PEG mold, and PEG was dissolved by soaking in water at room temperature to complete the bellows. Electrolysis actuators were assembled by filling the bellows with double distilled (DD) water and carefully mounting with the Nafion®-coated interdigitated Pt electrodes using laser cut double-sided pressure sensitive adhesive film (3 M™ Double Coated Tape 415, 3 M, St. Paul, MN). The seal was reinforced with marine epoxy (Loctite, Westlake, OH) (Sheybani et al. 2012b).

Dosing sensors were fabricated from 99.9 % Pt wire (Ø 0.5 mm) (California Fine Wire, Grover Beach, CA). A 2 mm segment of the tip was sanded (60 and 220 grit silicon carbide sandpaper) to increase surface area. The sensors were placed inside the vertical reservoir wall indentations, bent through the access ports, and soldered to Kynar™ silver plated copper wires (30 AWG, Jameco Electronics, Belmont, CA) to establish the electrical connection with the wireless circuit (Fig. 3a). Once in place, marine epoxy was used to create a water-resistant seal. The actuator was then incorporated into the reservoir using biocompatible epoxy (EPO-TEK® 730 unfilled, Epoxy Technologies, Billerica, MA).

Passive spring-loaded ball check valves were fabricated using custom-made parts. The valve housing consists of a valve stop and a valve seat produced using stereolithography (SL) in USP class VI DSM Somos® WaterShed XC 11122 material (FineLine Prototyping, Inc., Raleigh, NC). In order to improve sealing on the valve seat an o-ring was built as follows: a small amount of USP class VI silicone elastomer (MED-4210, Factor II, Inc., Lakeside, AZ) was poured directly into the valve seat using a pipette and cured at 40 °C. Once cured, the inner diameter of the membrane was cored using a 20 G needle. Compression springs were custom-made from high performance MP35N (nickel-cobalt-chromium-molybdenum) alloy with a spring rate of 0.035 N/mm (MDC 18725c, Motion Dynamics Corp., Fruitport MI). Stainless steel balls (Ø 1.587 mm, Ultra-Hard Wear-Resistant 440C Stainless Steel, no parting line) were purchased from McMaster-Carr (Elmhurst, IL). The last 2–3 coils of one end of the spring were opened to a larger diameter to allow the ball to connect to the spring without the need for any adhesives. The small diameter end of the microspring was placed on the valve stop and then the valve seat and valve stop were compression fit together. The valve was assembled without the use of adhesives (Fig. 3b). The final valve length was approximately 5.5 mm with a 2.6 mm outer diameter. Following characterization testing, the check valve was incorporated within the reservoir housing outlet, prior to the connection of the silicone delivery catheter (Fig. 3c).

The external and internal transceiver circuits were implemented as follows and fabricated on rigid and flexible printed circuit boards (PCBs), respectively (Fig. 4).

External Transceiver (Transmitter & Receiver) A 2 MHz clock oscillator (ECS −2100, ECS international, Olathe, KS), along with a quad bilateral switch (CD4016BC, Fairchild Semiconductor, San Jose CA) controlled by a resistor-set oscillator (LTC 6906, Linear Technologies, Milpitas, CA), were used to generate the power and sensing signals (500 kHz), respectively. The generated signal was then amplified in two stages before being applied to a tuned transmitting coil (8 turns of 20 AWG single strand wire, size: 310 mm × 140 mm). The signal received with the external receiving coil (8 turns of 20 AWG single strand wire, Ø 50 mm), was first filtered using a low pass elliptic filter (f_{cutoff}=1 MHz; LTC1560-1, Linear Technologies, Milpitas, CA) and then amplified using an LM7171 operational amplifier (Texas Instruments, Dallas, TX). The resulting signal was multiplied by the original 500 kHz transmitted signal (AD835, Analog Devices, Norwood, MA). The multiplier operates with 1 V input signals. A resistive voltage divider was used to decrease the amplitude of the 500 kHz signal before it was supplied to the multiplier. In order to reduce loading effects on the transmitted signal, a single inverter gate (SN74LVC1GU04DBVR, Texas Instruments, Dallas, TX) was used as a buffer between the two stage amplifier and the voltage divider.

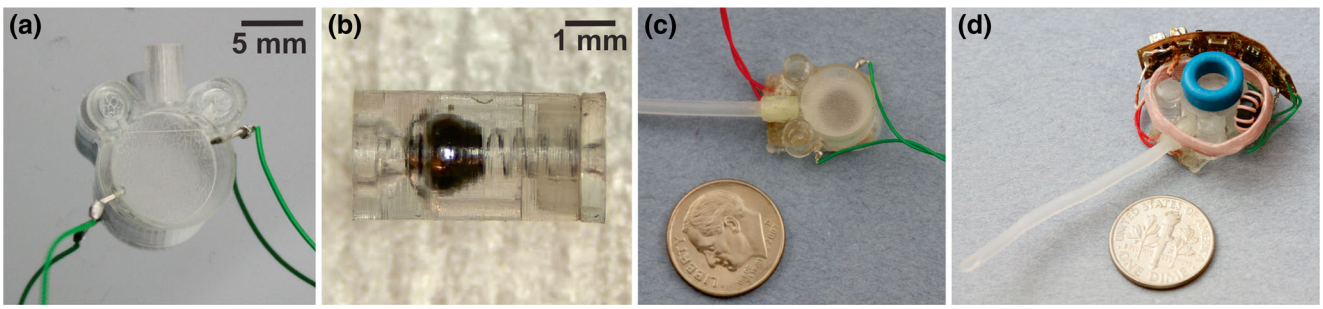

Fig. 3 Photographs of micropump assembly: **a** dosing sensors incorporated into the reservoir wall across from each other, **b** assembled check valve, **c** assembled micropump prior to the incorporation of circuit and coils, **d** micropump with integrated sensors and circuity

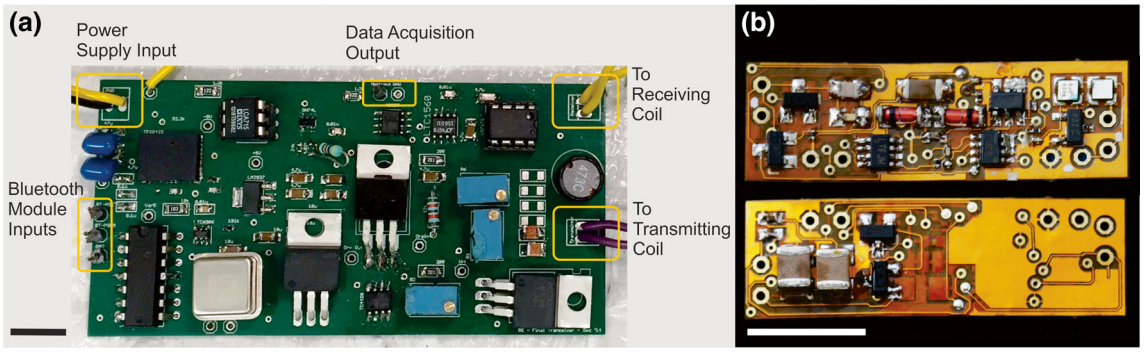

Fig. 4 Photograph of **a** external and **b** internal transceiver PCBs: top and bottom image show front and back of PCB, respectively. Scale bars represent 10 mm

Internal transceiver (transmitter & receiver) Litz wire (6 turns, 50/54 SPN/SN, Wiretron, Volcano, CA) was used for the receiving coil (Ø 22 mm). A ferrite toroid core (OD 10 mm, B64290L38X830, EPCOS AG, Munich, Germany) was added to the receiving coil to enhance coupling and increase voltage pick up (ferrite cores have been shown to conduct the flux lines through the center of the receiver and improve the coil coupling (Schuylenbergh and Puers 2009)). The internal transmitting coil (6 turns, L=110 μH at 500 kHz) was also fabricated using Litz wire (50/54 SPN/SN, Wiretron, Volcano, CA) wrapped around a ferrite core (toroid core, OD 6.3 mm, B64290P37X830, EPCOS AG, Munich, Germany). The core was used to produce larger inductances in a smaller space (Schuylenbergh and Puers 2009). The circuit components and the electrolysis micropump require a direct current (DC) power signal. Therefore, the received alternating signal was fully rectified using two Schottky diodes (BAT54A and BAT54C, Fairchild Semiconductor, San Jose, CA). A zener voltage regulator diode (BZV55, NXP Semiconductors, Eindhoven, Netherlands) was used to regulate the output voltage of the power signal. AD5227 (Analog Devices, Norwood, MA) was used as the current setting potentiometer to set the output current of the adjustable current regulator (LT3092, Linear Technology, Milpitas, CA). The infusion rate modulation signal was separated by half-wave rectification (BAT54A) and then filtered using a low pass RC design. A low frequency oscillator (LTC 6991, Linear Technology, Milpitas, CA) set the potentiometer clock frequency to 213 Hz. The modulation sensing signal was also separated by half-wave rectification (BAT54A). A zener voltage regulator diode (BZV55, NXP Semiconductors, Eindhoven, Netherlands) was used to limit the output voltage of the signal to prevent damage to the MOSFETs. An n-channel MOSFET (Si8424CDB, Vishay Siliconix, Singapore) was used as a voltage controlled variable capacitor and placed in parallel with the sensors. A p-channel MOSFET (Si8429DB, Vishay Siliconix, Singapore) and a BJT transistor (2 N4401, Fairchild Semiconductor, San Jose, CA), were used, in a source-follower buffer configuration, to maintain constant current through the sensors (~100 μA). The current value was chosen based on the expected sensor resistance range at the measurement frequency. The n-MOSFET capacitance was altered 2.5 – 1 nF for V_{DS}=0–2 V respectively. The current value was chosen so that the voltage across the sensors (and the MOSFET) varied between 0 and 2 V for expected sensor resistance range for the reservoir deliverable volume. The resistance range is dependent on the ionic conductivity of the drug fluid and the size of the reservoir.

3 Experimental methods

Medical devices and pharmaceutical therapies are typically first validated in animal models in early stage testing. The research prototype presented in this work (Fig. 3d) was scaled for small animals (rodents) which are a widely used animal model in drug discovery and development. The design targets use of the implanted infusion system in an animal housed inside a typical vivarium cage set that is situated inside the external transmitting coil. The external receiving coil is located on the cage wall perpendicular to the external transmitting coil.

3.1 Wireless flow control calibration

As mentioned in the design section, a Parallax Board of Education USB carrier board kit, a Basic Stamp 2 Module microcontroller, and an Easy Bluetooth Module (Parallax Inc., Rocklin, CA) were used to control wireless signal transmission from the external module to the internal circuit via Bluetooth. LabVIEW (v 2009, National Instruments, Austin, TX) and Basic Stamp 2 Editor (v. 2.5.2) were utilized to program the communication and signal processing functions. The communication requires the pulse width of the ASK signal to be >15 mS. Due to this

timing limitation, the frequency of the internal clock was set to 213 Hz. Theoretical output current values were calculated based on equations provided in the potentiometer (1) and current regulator datasheets (2, 3):

$$\Delta R = (CP \times (5\ k\Omega)/64 + 70\ \ \Omega) \quad (1)$$

where CP is the number of clock pulses.

$$R_{ext} = (5\ k\Omega - \Delta R) \| 750\ \Omega \quad (2)$$

$$I_{out} = (80\ k\Omega)/R_{ext} \times 10\ \mu A \quad (3)$$

The program was then tested by using a 1 kΩ load in place of an actuator and calculating the output current by measuring the voltage across the load. The current was increased in discrete incremental steps.

The circuit was then connected to the micropump and the program was used to increase the output current in incremental steps. 10× PBS was used as the drug model, and the infusion flow rate was calculated by measuring fluid front movement in a calibrated 50 μL micropipette connected to the outlet of the micropump (n=4).

3.2 Wireless sensing calibration

The micropump was filled with 10× PBS as a model drug and the integrated dosing sensors were connected to the internal circuit. For each run, eight consecutive boluses (~5.33 μL per bolus) were delivered (1 mA current applied using a Keithley 2400 sourcemeter, Keithley Instruments Inc., Cleveland, OH). The volume dispensed from the pump was calculated based on fluid front movement in a calibrated 100 μL micropipette attached to the micropump catheter outlet. The sensor signal was recorded prior and after each bolus delivery and normalized to the baseline value for each run (measured value prior to first bolus delivery, n=4).

3.3 Simultaneous wireless flow control and sensing

An example regimen was chosen to demonstrate real-time wireless flow rate variations and simultaneous dose sensing for a micropump (prior to the integration of the check valve; 2 devices, n=2 per device). The micropump reservoir was filled with 10× PBS. The LabVIEW interface was used to select 1.04, 0.28, 0.52, 0.14, 0.83, and 1.04 μL/min as the expected output flow rates. Each flow rate selection lead to current application to the electrolysis electrodes. Pumping durations were selected to be 2, 7, 1.5, 8.75, 4, and 3 min, respectively. The sensor response was recorded before and after each delivery and then analyzed using the LabVIEW graphical user interface according to the calibration curve obtained, and an estimation of the delivered volume based on the calibration curve was presented to the user following each delivery. Between each run, complete recombination was allowed to occur and the reservoir was refilled.

3.4 Recombination detection

Once the current application to the electrolysis actuator ceases, gases generated by the bellows actuator recombine back to water and in the absence of a flow regulating check valve in-line with the delivery catheter, dispensed drug along with bodily fluids will be retracted into the catheter and potentially inside the pump during the recombination process thereby impacting the accuracy of dosing. Therefore, tracking this phenomena with the dosing sensors is desirable to improve dosing accuracy. However, as recombination occurs on a much slower time scale compared to actuation, drift may dominate the EI measurement.

In order to determine the feasibility of detection of recombination processes using wireless dosing sensors, the outlet of the micropump filled with 10× PBS was attached to a 100 μL calibrated micropipette. Generated gas volume and recombination were indirectly measured by observing the fluid front movement in the micropipette. A 43 μL bolus was delivered, the current was turned off, and recombination was measured periodically based on the fluid back flow in the micropipette for 60 min. At each measurement time point wireless dose sensing was used to estimate the volume of fluid in the reservoir. This value was subtracted from the total delivered volume to attain the recombined volume. These results were then compared to the visually observed recombination in the micropipette (n=3).

During EI measurements, each time the sensing signal is applied to the sensors, the electrochemical cell is perturbed and depending on the excitation voltage used to obtain the measurement, a finite amount of time is required for the system to settle into equilibrium (Kaisare et al. 2011). Drift measurement studies using a precision LCR meter directly connected to the dosing sensors had shown that the majority of drift is observed within the first hour until a state of equilibrium is reached (data not shown). Based on these results, another experiment was performed in which an 11.52 μL bolus of 10× PBS was delivered using the micropump attached to a 50 μL calibrated micropipette. The system was left unperturbed for two hours before wireless dose sensing was used to estimate the volume of fluid in the reservoir.

3.5 Check valve characterization

The valve was first characterized with a custom pressure setup in order to obtain an initial operating range (3 check valves, n=4 runs per check valve). Pressurized water was applied to the inlet of the valve in increments of 2.6 mmHg (0.05 psi,

0.34 kPa) from 0 mmHg until water flow was observed to determine cracking pressure. Reverse pressure was investigated by applying the pressurized water to the valve outlet. In order to avoid stiction, valves were flushed prior to each run.

The check valve was then incorporated into a wired micropump at the reservoir outlet and characterized. Forward flow rate and reverse leakage were measured by monitoring fluid front movement in a 100 μL calibrated micropipette attached to the valve outlet. 0.5 mA current was applied to the actuator using a Keithley 2400 sourcemeter (Keithley Instruments Inc., Cleveland, OH) to deliver 30 μL after valve opening was observed. Current was turned then off and fluid front movement in the micropipette was monitored for an hour after each run to determine valve reverse leakage (3 check valves, n=4 runs per check valves). Flow performance of the same valve-less pump served as a control.

3.6 Valved system operation

Following the incorporation of the check valve in the fully integrated wireless system, once again a realistic drug regimen was selected to characterize system performance (Cobo et al. (2015)). The micropump reservoir was filled with 10× PBS. The LabVIEW interface was used to select 1.04 μL/min as the expected output flow rate. A 50 μL calibrated micropipette was connected to the valve outlet to quantify fluid front movement. The flow rate selection initiated current application to the electrolysis electrodes in 1 min increments until fluid flow was observed.

A larger commercially-available spring-loaded ball check valve (Model #101, Smart Products, Morgan Hill, CA; Ø 4.57 mm, length=9.53 mm) with a cracking pressure of 0.58 psi (30 mmHg, 4.0 kPa) was then inserted in place of the custom-made check valve. Once again, the micropump reservoir was filled with 10× PBS. The LabVIEW interface was used to select 1.04 μL/min as the expected output flow rate. A 50 μL calibrated micropipette was connected to the valve outlet to quantify fluid front movement. The flow rate selection initiated current application to the electrolysis electrodes in 1 min increments until fluid flow was observed. Following the observation of flow (denoting valve opening), 1.04 μL/min was selected as the expected output flow rate for three 1 min durations, followed by the selection of 0.28 μL/min for three 1.5 min durations. The sensor response was recorded before and after each bolus delivery and then analyzed using the LabVIEW graphical user interface according to the calibration curve obtained and an estimation of the delivered volume based on the calibration curve was presented to the user following each delivery. Following the completion of the regimen, the current application was seized and reverse leakage during recombination was observed for an hour.

3.7 Effects of coil misalignment on power and data transfer

Wireless inductive transmission has some limitations, such as short operating range and the need for alignment between coils (Zhang et al. 2009). The micropump presented in this work is meant to be implanted in a freely moving subject. If the transmitting and receiving coils are oriented perpendicularly to one another, then the mutual inductance would be zero and essentially no power would be transmitted (Lenaerts 2008). Therefore, it is important to characterize the effects of coil separation distance and coil misalignment in power transmission and sensing and account for power transmission losses in the wireless system design.

Variations in the output current, as a result of decreased power transfer with increasing distance and misalignment between the external transmitting and internal receiving coil, were calculated by measuring the voltage across a 1 kΩ test load.

3.8 Delivery in simulated brain tissue material

Preliminary results for successful power transmission through the simulated brain tissue material were previously demonstrated (Sheybani and Meng 2014). The results showed no significant difference between infusion flow rates for wireless transmission through air vs. simulated tissue; one way analysis of variance, $p<0.05$). In order to mimic the effects of wireless data transmission through tissue, simulated brain tissue was prepared according to the recipe described in (Hartsgrove et al. 1987). Briefly, sugar, NaCl salt, and Natrosol® (hydroxyethylcellulose, Ashland Inc., Covington, KY) were dissolved in 800 mL of DD water (1108.9, 49.5, and 19.8 g, respectively). 1.98 g of ProClin® 950 preservative (Sigma-Aldrich, St. Louis, MO) was added as a replacement for Dowicil 75® (1-(3-chloroallyl)-3, 5, 7-1-(3-chloroallyl)-3, 5, 7-triaza-1-azonia adamantane chloride). A 4 cm thick slab of gel-like material was created for testing. The micropump reservoir was filled with 10× PBS mixed with blue food coloring to enhance visual contrast during delivery. Then the pump and circuit were then placed inside the simulated brain tissue so that each transmitting and receiving coil pair was separated by 2 cm of the simulated tissue. Delivery at the catheter outlet was recorded using a Canon digital single lens reflex (SLR) camera (EOS Rebel XSi, Canon, Tokyo, Japan). After placement, the catheter outlet was monitored for 2 min, to observe potential diffusion of the reservoir contents into the simulated tissue material. The LabVIEW interface was then used to select 0.52 and 1.04 μL as the expected output flow rates. Each flow rate selection lead to current application to the electrolysis electrodes. Pumping durations were selected to be 4 and 3 min, respectively. The sensor response was recorded periodically and analyzed using the LabVIEW graphical user

interface according to the calibration curve and an estimation of the delivered volume based on the calibration curve was calculated at each measurement time point.

4 Experimental results

4.1 Wireless flow control calibration

The following four output current values were achieved: 0.465, 0.485, 0.530, 0.55, and 0.6 mA by measuring the voltage across the 1 kΩ load in place of the actuator.

Figure 5 shows the variable current results with the infusion pump. The measured flow rate (0.14 – 1.04 μL/min) closely followed the changes in current initiated using the interface program. It is important to note that other current values (between 0.465 and 0.6 mA) and therefore flow infusion rates (between 0.14 and 1.04 μL/min) can be achieved by altering the ASK data signal pulse width.

4.2 Wireless sensing calibration

Figure 6a shows the results for the four runs that were then used to obtain averaged trends. Sensor response values for each trace were normalized to the value measured for the full reservoir. The following relationships exist between the parameters used for wireless sensing (4, 5, 6, 7):

$$\Delta Volume \propto \Delta R_{sensor} \tag{4}$$

$$\Delta R_{sensor} \propto \Delta V_{MOSFET} \tag{5}$$

$$\Delta V_{MOSFET} \propto e^{-\Delta C_{MOSFET}} \tag{6}$$

$$\frac{1}{\sqrt{\Delta C_{MOSFET}}} \propto \Delta f_{res} \propto \Delta sensor\ response \tag{7}$$

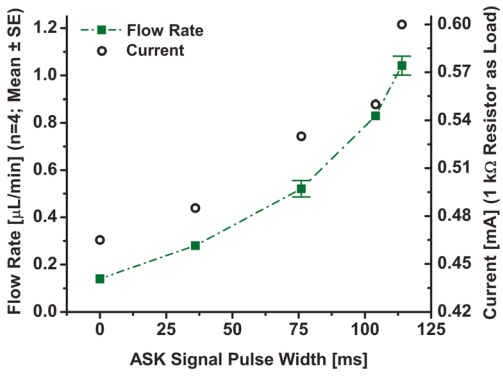

Fig. 5 Five step incremental increase in receiver current output measured across a 1 kΩ resistor and the micropump (at each modification step, a specific pulse width was applied to achieve the desired change in the wiper position)

Using these relationships, a linear relationship can be obtained between the volume delivered from the micropump and the sensor response (8):

$$\Delta Volume \propto -\ln\left(\left(\frac{1}{\Delta sensor\ response}\right)^2\right) \tag{8}$$

The averaged results from the calibration tests were then used to obtain this linear relationship and calibration curve between the volume delivered by the micropump and the natural log of the sensor response (Fig. 6b). This curve was subsequently used to program the LabVIEW graphical user interface to estimate the volume delivered by the micropump with an accuracy of ±10 %.

It should be noted that as sensor response is dependent on the cross sectional area of the fluid contained in the reservoir, the calibration curve will be identical for different reservoir sizes if bolus delivery is normalized to the reservoir fill volume.

4.3 Simultaneous wireless flow control and sensing

The results for real-time wireless flow rate variations and simultaneous dose sensing for the micropump are presented in Fig. 7 as a comparison between the programmed volume (based on the selected flow rate and delivery duration), the sensed volume (based on analysis of the sensor response), and the actual delivered volume as calculated from fluid movement in a calibrated 50 μL micropipette connected to the micropump catheter outlet. The smallest volume delivered during this test was 0.55 μL boluses which constitutes ~0.3 % of the micropump's deliverable volume and ~0.13 % of the reservoir's fill volume. However, this resolution can only be attained if the accumulated delivered volume since the last refill is>2 μL. The non-linear relationship between the sensor response and delivered volume (8) leads to increased sensitivity (and bolus resolution) as accumulated volume increases.

4.4 Recombination detection

Approximately 30 % of the delivered volume recombined within 12 min, this volume was correctly estimated using the dosing sensors within ±15 %. Drift in measurement dominated the remainder of recombination and the volumes could not be correctly estimated.

For the unperturbed system within two hours, the recombined volume was estimated to be 2.03 μL, approximately 26 % less than the recombined volume calculated from fluid backflow in the micropipette (2.78 μL). The results are promising, especially if the speed of recombination is increased by increasing the available catalyst surface area in the electrolysis chamber. It may be possible to estimate recombination at certain time points following delivery.

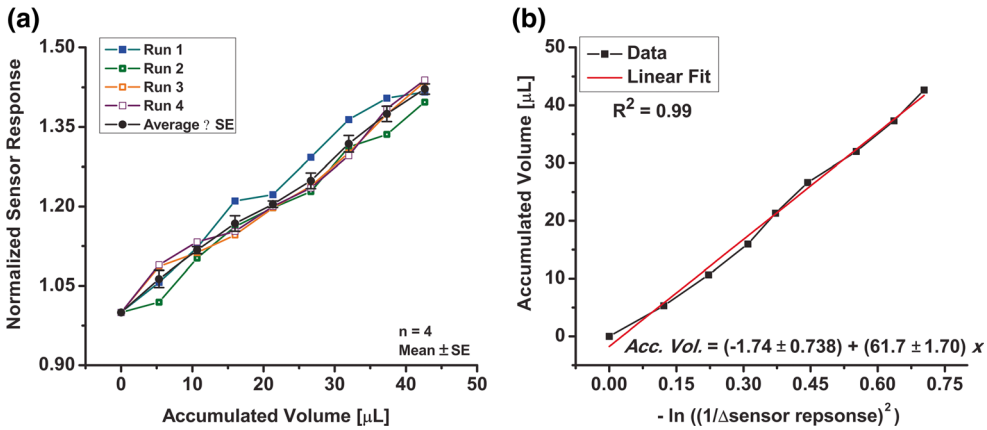

Fig. 6 **a** Calibration testing for wireless sensing: 8 boluses, each 5.33 μL (1.33 % of reservoir fill volume) delivered for each of the four runs. **b** Averaged results from calibration tests were used to obtain a linear relationship between the volume delivered by the micropump and the natural log of the sensor response

4.5 Check valve characterization

The cracking pressure for the 3 tested check valves using the custom pressure setup were determined to be 1.46 (75.50, 10.07), 3.45 (178.42, 23.79), and 2.0 (103.43, 13.79) psi (mmHg, kPa), respectively (mean value for n=4 runs per check valve). Differences in cracking pressures can be attributed to manual fabrication and the tolerance of the stereolithography parts. No reverse leakage was observed for any of the three valves tested up to 4 psi (206.86 mmHg, 27.58 kPa). This pressure far exceeds values expected to be encountered during recombination and within various compartments of the body (Goers 2008).

The results for the characterization of valve #1 are presented in Fig. 8 (representative of the operation of all three valves). As expected, the time required to open each valve varied with the cracking pressure of valve tested. However, all three valves opened within one minute of micropump actuation. Once open, the valves did not present significant flow resistance to flow from the micropump. Yet, up to 13 % variability was observed between flow rates obtained in the four runs for each valve. Less than 1 % reverse leakage was observed for any of the three valves during recombination (n=4 for each valve).

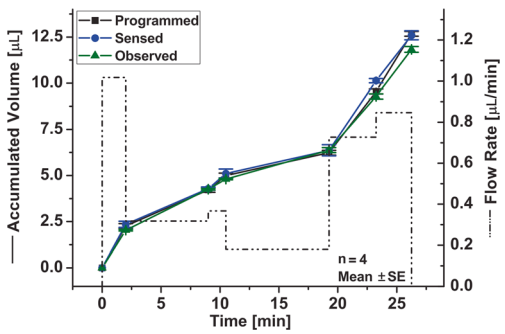

Fig. 7 Simultaneous wireless flow control and dose sensing for an example dosing regimen, comparing the expected delivered volume (based on the selected flow rate and delivery duration), the estimated delivered volume (based on analysis of the sensor response), and the actual delivered volume by the micropump

4.6 Valved system operation

After five minutes of consecutive actuation, no fluid flow was observed in the calibrated micropipette, suggesting that the cracking pressure of the custom-made check valve was too high to be overcome by the fully integrated wireless system. Given the long lead time to procure custom stereolithography parts for the custom-made check valves, a larger commercial valve with a lower cracking pressure was used to demonstrate the operation of the fully integrated system.

The results of system operation with the commercially available check valve are presented in Fig. 9. The valve opened after 63 s of actuation. Following valve opening, bolus volumes and flow rates sensed (based on analysis of the sensor response) and observed in the calibrated micropipette were comparable to those achieved without the check valve and no flow restrictions were observed. However, the check valve did not prevent reverse flow during recombination and the entire delivered volume was pulled back towards the reservoir.

4.7 Effects of coil misalignment on power and data transfer

The output current, calculated by measuring the voltage across a 1 kΩ load used in place of an actuator, was unaltered when the receiving coil was placed within±2.5 cm of the transmitting coil. Based on these results, for animal studies, the cage (e.g., polycarbonate reusable animal cage, 23.8×13.8×13 cm^3, Tecniplast, Buguggiate, Italy) should be placed inside the transmitting coil, with the coil ~2.5 cm from the bottom edge of the cage allowing for proper delivery within 5 cm of the cage bottom. Unaltered transmission was observed for 5° misalignment between coils placed 2 cm apart. 10° misalignment between coils placed at the same distance lead to 7 % drop in the received current. Current control could not be achieved for misalignment angles >15°.

For wireless sensing, the multiplier on the external transmitter operates with 1 V input signals. The received

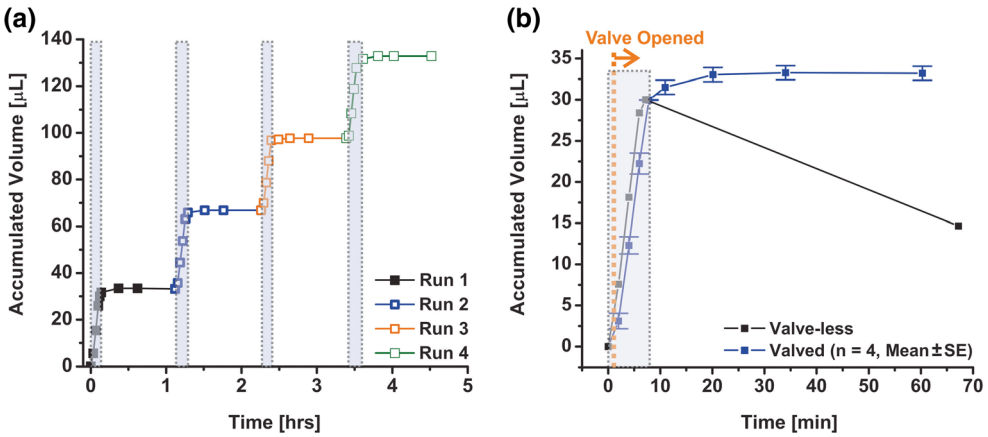

Fig. 8 Valve characterization with wired micropump: **a** four 30 μL boluses delivered after valve opening (micropump was refilled after each run to circumvent pressure buildup during recombination), **b** Valve performance averaged for the four runs and compared to a valve-less system (the dashed orange line shows check valve opening; shaded areas in both graphs represent active pumping)

signal was filtered and then amplified prior to multiplication. A potentiometer was used to set the amplifier gain. For sensing presented here, the gain was chosen to allow for up to 5 cm of distance between the internal transmitting and external receiving coils. The transmitter gain can be adjusted to accommodate increased distance between the coils. However, it is important to note, that for inductive transmission, the receiving coil should be placed within the inductive field created by the transmitting coil (Schuylenbergh and Puers 2009). As such, when implanted in a moving subject, the external receiving coil (Ø 50 mm presented here) may have to be moved along with the moving animal. Kilinc, et al., have developed a servo-controlled system that could track an animal's movements and move an external coil accordingly (Kilinc et al. 2014). If needed, a similar setup could be used to automate moving of the receiving coil based on the movement of the internal transmitting coil. Alternatively, a larger external receiving coil could be used that would accommodate movement within the entire cage.

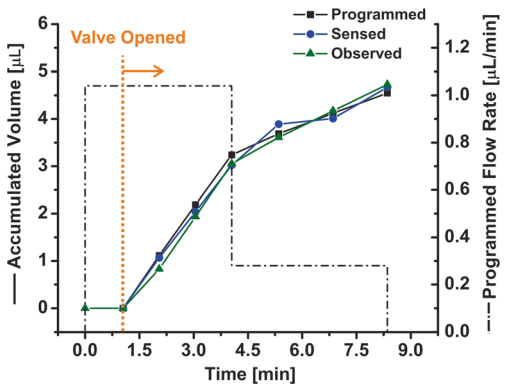

Fig. 9 Simultaneous wireless flow control and dose sensing for an example dosing regimen for a system with an integrated commercially-available check valve, comparing the expected delivered volume (based on the selected flow rate and delivery duration), the estimated delivered volume (based on analysis of the sensor response), and the actual delivered volume by the micropump. The dashed orange line shows the onset of delivery due to the opening of the valve

4.8 Delivery in simulated brain tissue material

No diffusion was observed from the catheter outlet prior to active delivery from the micropump. Screen grabs of the recorded video are shown in Fig. 10. Successful wireless infusion flow control and sensing was achieved in the simulated brain tissue material. Image analysis using ImageJ software (National Institutes of Health) confirmed that flow rate was successfully altered.

5 Discussion

Drug delivery is essential for the treatment of chronic diseases. Implantable site-specific drug delivery devices can deliver a potent and effective dose of drug directly to the site of therapy, improving treatment outcomes while reducing potential side effects and the risk of infection due to catheters running across the skin. These factors serve to increase patient comfort and decrease overall associated healthcare costs for the treatment of chronic conditions. A microelectromechanical systems approach to the design and fabrication of such devices miniaturizes infusion pumps such that they are implantable; wirelessly powered to eliminate the use of bulky, limited lifetime batteries; and volume efficient. Wireless data communication allows device status and performance to be monitored remotely as well as remotely initiated changes to the drug regimen by caregivers throughout the course of treatment to tailor the drug regimen to the individual needs of each patient.

The fully integrated wireless system presented here combines an electrolysis-based micropump with the electrochemical dose tracking system and is scaled for small animal (rodents) research. The final prototype with the integrated coils and circuitry weighed 4.1 g (for a micropump with an empty reservoir). An adult male mouse and rat weigh approximately 30 and 400 g, respectively (The Johns Hopkins University 2015). As such the implantable prototype should weigh <10 % of the animal's body weight (3 g for use in mice and 40 g for use in rats).

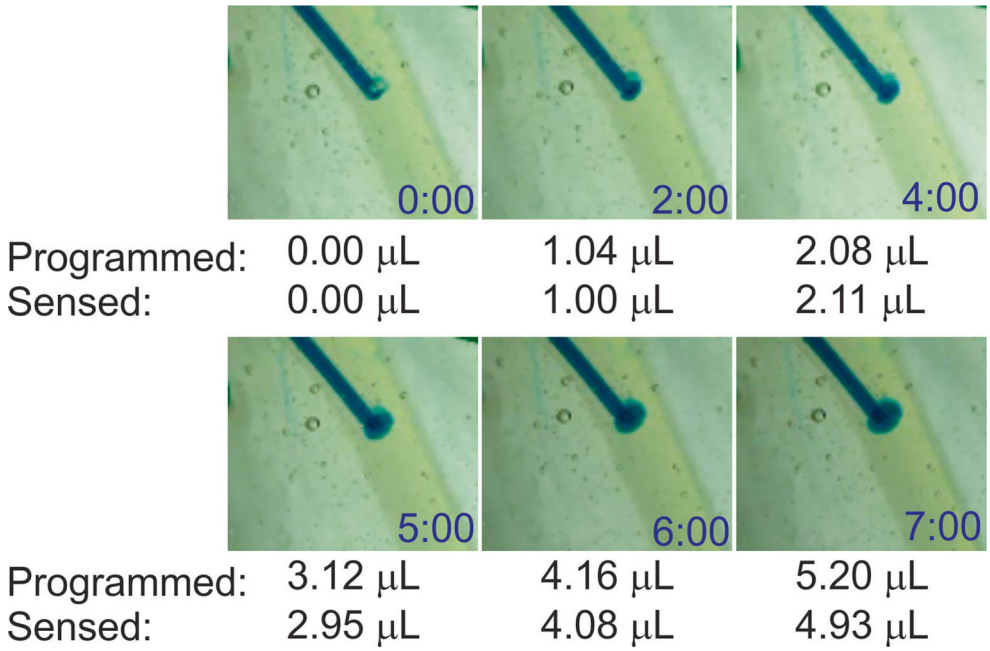

Fig. 10 Photographs showing delivery of 10× PBS mixed with blue food coloring in simulated brain tissue material. The programmed volume (based on the selected flow rate and delivery duration) and the sensed volume (based on analysis of the sensor response) are included at each time point (minutes:seconds)

Due to the chronological nature of system design, several restrictions were placed on the performance of the final prototype that could be mitigated through future work. The output current range (and as a result the infusion flow rate), as well as, the allowable coil misalignment and distance were limited compared to that attained previously for the micropump without the integrated sensors (Sheybani and Meng 2014). This can be attributed to decreased power transfer efficiency when the power signal is modulated with the sensing signal and could potentially be mitigated by redesigning the system to increase power amplification, including multiple receiving coils, or increasing the operation frequency of the sensing signal. As a result of the lower current range, the cracking pressure of the custom-made check valve was too high to be overcome by the fully integrated wireless system in a timely fashion (within 5 min). Given the long lead time to procure custom parts for the custom-made check valves, a larger commercial valve with a lower cracking pressure was used to provide a demonstration of the potential of the fully integrated system. The finite time required to open the valve by overcoming the cracking pressure can be compensated, in part, by tracking the doses using the integrated sensors and adjusting the duration that the pump is activated accordingly. For applications in which lower flow rates and near instantaneous delivery in a smaller pump package are required, an improved custom-made valve with a lower cracking pressure would need to be designed.

Lastly, static tissue models may not fully capture wireless power transfer and sensing in live moving animals. While efforts were taken to simulate operation and proper function of the system in a moving subject, a true test of functionality would require implantation in animal models. However, prior to animal testing, the power transfer and allowable coil misalignment would have to be increased.

Despite these shortcomings, the high-performance drug delivery micropump presented offers the potential for unprecedented accuracy in delivering a diverse assortment of liquid drug formulations at the right dose, to the right tissue, and at the right time over the entire course of treatment. Wireless flow controllability and dose tracking sensors, improve patient safety and allow for active control over the delivery profile and early warning of pump malfunctions leading to optimized and personalized patient-tailored therapy.

6 Conclusion

A fully integrated wireless, programmable, implantable electrolysis-based micropump with incorporated EI dosing sensors was presented. Wireless inductive powering and data telemetry (through amplitude and frequency modulation) were utilized to achieve variable flow control and data transmission to and from the sensors. Wireless infusion rate control (0.14–1.04 μL/min) and dose sensing (bolus resolution of 0.55–2 μL) were each calibrated separately with the final circuit architecture and then simultaneous wireless flow control and dose sensing was demonstrated for an example delivery regimen. Using the dosing system recombination of gases and the resulting fluid retraction was measured within±26 %. A custom-made normally closed spring-loaded ball check valve was designed and incorporated at the reservoir outlet to prevent backflow of fluids as a result of the reverse pressure gradient caused by recombination. The check valve was successfully characterized using wired micropump with <1 %

reverse leakage. However, the cracking pressure of the custom-made check valve was too high to be overcome by the fully integrated wireless system in a timely fashion due to the drop in output current level resulting from the integration of both wireless sensing and power transfer. The effects of coil distance and misalignment in wireless power and data transfer were also studied. Successful delivery, infusion rate control, and dose sensing was achieved through simulated brain tissue material.

Future work includes increasing the attainable output current range and allowable coil misalignment through redesigning the amplification portion of the wireless transmitter or increasing the operation frequency of the sensing signal.

Acknowledgments This work was supported by National Science Foundation accelerating innovation research – technology translation (NSF AIR- IIP 1343467) and National Institutes of Health (NIH - R21 GM104583) funding sources. The authors thank the members of the USC Biomedical Microsystems Laboratory for their assistance. E. Meng has a significant financial interest in Fluid Synchrony LLC.

References

B. Bruguerolle, G. Labrecque, Rhythmic pattern in pain and their chronotherapy. Adv. Drug Deliv. Rev. **59**(9–10), 883–895 (2007)

A.M. Cobo, R. Sheybani, H.M. Tu, E. Meng, A wireless implantable micropump for localized drug infusion. Sensors Actuators A. Phys. (2015 *(submitted)*)

FDA: US Food and Drug Administration, Medtronic Model 8637 SynchroMed II Implantable Infusion Pump. (2011) Medical Device Recalls, from http://www.fda.gov/MedicalDevices/Safety/ListofRecalls/ucm271492.htm

FDA: US Food and Drug Administration, Medtronic SynchroMed II implantable drug infusion pump and SynchroMed EL implantable drug infusion pump. (2012). Medical Device Recalls Retrieved 3/25/2012, from http://www.fda.gov/MedicalDevices/Safety/ListofRecalls/ucm333231.htm

FDA: US Food and Drug Administration, Roche insulin delivery systems, ACCU-CHEK FlexLink plus infusion sets. (2011) Medical Device Recalls Retrieved 5/10/2013, from http://www.fda.gov/MedicalDevices/Safety/ListofRecalls/ucm248772.htm

FDA: US Food and Drug Administration, SIGMA spectrum infusion pump Model 35700 - expanded recall. (2011) Medical Device Recalls, 5/10/2011, from http://www.fda.gov/MedicalDevices/Safety/ListofRecalls/ucm308488.htm

J. Fiering, M.J. Mescher, E.E. Leary Swan, M.E. Holmboe, B.A. Murphy, Z. Chen, M. Peppi, W.F. Sewell, M.J. McKenna, S.G. Kujawa, J.T. Borenstein, Local drug delivery with a self-contained, programmable, microfluidic system. Biomed. Microdevices **11**(Compendex), 571–578 (2009)

H.M. Gensler, A wireless implantable MEMS micropump system for site-specific anti-cancer drug delivery (University of Southern California, 2013)

H. Gensler, R. Sheybani, E. Meng, Rapid non-lithography based fabrication process and characterization of Parylene C bellows for applications in MEMS electrochemical actuators. 16th International Solid-State Sensors, Actuators and Microsystems Conference, Transducers'11, Beijing, China, IEEE Computer Society, 2011.

T.A. Goers, The Washington manual of surgery (Lippincott Williams & Wilkins, 2008)

F. Halberg, E. Haus, S. Cardoso, L. Scheving, J. Kühl, R. Shiotsuka, G. Rosene, J. Pauly, W. Runge, J. Spalding, Toward a chronotherapy of neoplasia: tolerance of treatment depends upon host rhythms. Cell. Mol. Life Sci. **29**(8), 909–934 (1973)

E. Halberg, G. Cornelissen, F. Halberg, Optimization of the chronotherapeutic index in the experimental animal laboratory. In Vivo (Athens, Greece) **6**(4), 371 (1992)

G. Hartsgrove, A. Kraszewski, A. Surowiec, Simulated biological materials for electromagnetic radiation absorption studies. Bioelectromagnetics **8**(1), 29–36 (1987)

W. Hrushesky, Cancer chronotherapy: a drug delivery challenge. Prog Clin Biol Res A **341**, 1–10 (1990)

N.S. Kaisare, V. Ramani, K. Pushpavanam, S. Ramanathan, An analysis of drifts and nonlinearities in electrochemical impedance spectra. Electrochim. Acta **56**(22), 7467–7475 (2011)

E.G. Kilinc, K. Kapucu, F. Maloberti, C. Dehollain, Servo-controlled remote powering and low-power data communication of implantable bio-systems for freely moving animals. Biomedical Circuits and Systems Conference (BioCAS), 2014 IEEE, 2014

B. Lenaerts, *Omnidirectional inductive powering for biomedical implants* (Springer, New York, 2008)

C.G. Lis, J.F. Grutsch, P. Wood, M. You, I. Rich, W.J.M. Hrushesky, Circadian timing in cancer treatment: the biological foundation for an integrative approach. Integr Cancer Ther **2**(2), 105–111 (2003)

K. Menehan, Partnership for solutions: better lives for people with chronic conditions. National Program Report. M. B. Janet Heroux, Robert Wood Johnson Foundation, 2006

E. Meng, T. Hoang, MEMS-enabled implantable drug infusion pumps for laboratory animal research, preclinical, and clinical applications. Adv. Drug Deliv. Rev. (2012)

D. Paolino, P. Sinha, M. Fresta, M. Ferrari, Drug delivery systems. Encycl. Med. Devices Instrum. (2006)

K.V. Schuylenbergh, R. Puers, *Inductive powering : basic theory and application to biomedical systems* (Springer, Dordrecht, 2009)

R. Sheybani, E. Meng, High-efficiency MEMS electrochemical actuators and electrochemical impedance spectroscopy characterization. J. Microelectromech. Syst. **21**(5), 1197–1208 (2012)

R. Sheybani, N.E. Cabrera-Munoz, T. Sanchez, E. Meng, Design, fabrication, and characterization of an electrochemically-based dose tracking system for closed-loop drug delivery. Engineering in Medicine and Biology Society (EMBC), 2012 annual international conference of the IEEE (2012)

R. Sheybani, H. Gensler, E. Meng, A MEMS electrochemical bellows actuator for fluid metering applications. Biomed. Microdevices (2012) 1–12

R. Sheybani, S. Elyahoodayan, E. Meng. Closed-loop on-demand drug delivery micropump for chronic pain management applications. 7th international conference on microtechnologies in medicine and biology (MMB'13), Marina Del Rey, CA. 2013

R. Sheybani, E. Meng, On-demand wireless infusion rate control in an implantable micropump for patient-tailored treatment of chronic conditions. Engineering in Medicine and Biology Society (EMBC), 2014 36th Annual International Conference of the IEEE, 2014

R. Sheybani, E. Meng, A wireless implantable drug infusion system with integrated dosing sensors. The 18th international conference on solid-state sensors, actuators, and microsystems (Transducers'15), Anchorage, AK, USA, 2015

The Johns Hopkins University, Animal care and use committee: the mouse [and] the rat. (2015) Retrieved 3/1/2015, from http://web.jhu.edu.libproxy.usc.edu/animalcare/procedures/.

D.J.H. Tng, R. Hu, P. Song, I. Roy, K.T. Yong, Approaches and challenges of engineering implantable microelectromechanical systems (MEMS) drug delivery systems for *in vitro* and *in vivo* applications. Micromachines **3**(4), 615–631 (2012)

N. Trombly, Emerging technologies ehance drug delivery efficacy. (Medical Electronics Design, UBM Canon, 2012).

J. Urquhart, Controlled drug delivery: therapeutic and pharmacological aspects. J. Intern. Med. **249**(S741), 75–94 (2001)

J. Urquhart, J.W. Fara, K.L. Willis, Rate-controlled delivery systems in drug and hormone research. Annu. Rev. Pharmacol. Toxicol. **24**(1), 199–236 (1984)

B.-B.C. Youan, Chronopharmaceutics: gimmick or clinically relevant approach to drug delivery? J. Control. Release **98**(3), 337–353 (2004)

F. Zhang, L. Xiaoyu, S.A. Hackworth, R.J. Sclabassi, S. Mingui, *In vitro* and *in vivo* studies on wireless powering of medical sensors and implantable devices. 2009 IEEE/NIH Life Science Systems and Applications Workshop (LiSSA 2009), Piscataway, NJ, USA, IEEE, 2009.